Microchimica Acta (2019) 186: 629
https://doi.org/10.1007/s00604-019-3742-9

ORIGINAL PAPER

Laser-induced breakdown spectroscopy as a novel readout method for nanoparticle-based immunoassays

Pavlína Modlitbová[1] · Zdeněk Farka[2] · Matěj Pastucha[2] · Pavel Pořízka[1] · Karel Novotný[3] · Petr Skládal[2] · Jozef Kaiser[1]

Received: 28 February 2019 / Accepted: 7 August 2019 / Published online: 16 August 2019

Abstract

Laser-induced breakdown spectroscopy (LIBS) was examined as a novel method for readout of microtiter plate immunoassays involving nanoparticles (NP). The so-called Tag-LIBS technique is a sensitive method for the detection of specific biomarkers. It was applied to the determination of NP labels using nanosecond ablation sampling. The NP labels were examined from the bottom of a standard 96-well microtiter plate. Thanks to the flexibility of LIBS instrumentation, both the plasma emission collection and the focusing optics arrangements can be collinearly arranged. The experiments showed that silver NPs and gold NPs can be readily quantified on the bottom of the microtiter plate. Utilizing this technique, a sandwich immunoassay for human serum albumin using streptavidin-coated AgNP labels was developed. The assay has a 10 ng·mL^{-1} detection limit which is comparable to the sensitivity of fluorometric readout. The main advantage of this LIBS technique is its wide scope in which it enables a detection of almost any type of NP labels, irrespective to any fluorescence or catalytic properties. Owing to the immediate signal response, the relatively simple instrumentation also enables assay automation. The LIBS capability of multi-elemental analyses makes it a promising and fast alternative to other readout techniques, in particular with respect to multiplexed detection of biomarkers.

Keywords Collinear plasma collection · Gold nanoparticles · Laser ablation · Microtiter plate · Sandwich immunoassay · Silver nanoparticles · Streptavidin · Tag-LIBS

Highlights
- LIBS is a suitable readout method for nanoparticle-based immunoassays.
- Collinear LIBS arrangement for collection of plasma emission from the bottom of the standard 96-well microtiter plate was presented.
- Tag-LIBS was employed in a sandwich immunoassay for the detection of human serum albumin.

✉ Pavlína Modlitbová
Pavlina.Modlitbova@ceitec.vutbr.cz

[1] Central European Institute of Technology (CEITEC), Brno University of Technology, Technická 3058/10, 616 00 Brno, Czech Republic

[2] Central European Institute of Technology (CEITEC), Masaryk University, Kamenice 5, 625 00 Brno, Czech Republic

[3] Department of Chemistry, Faculty of Science, Masaryk University, Kotlářská 2, 611 37 Brno, Czech Republic

Introduction

Immunochemical assays combine the specificity of immunoreagents and the variation in detection approaches enabled by the use of different labels. The assays are usually based on the attachment of one of the immunoreagents to a solid phase and a subsequent addition of reagents that bind to each other (heterogeneous format). The bound and the free components are separated through washing steps [1]. The most widespread assay type – enzyme-linked immunosorbent assay (ELISA) – involves an antibody (or antigen) labeled with enzymes such as horseradish peroxidase or alkaline phosphatase. This labeling enables a quantification via the conversion of suitable substrate to a colored or fluorescent product [2]. The main advantages of enzymatic labels are the easy conjugation with antibodies and the high catalytic activity providing the amplification (a single enzyme molecule

converts multiple substrate molecules). However, when the enzymes are used as labels, they suffer several disadvantages including the high production costs, limited stability, and time-consuming signal development [3].

The progress in nanotechnology has led to a development of various nanomaterials that can be used to overcome the limitations of enzymes and to improve the assay properties. The applications of nanoparticle (NP) labels in immunoassays can be divided into two main categories: (a) catalytic nanoparticles (nanozymes), and (b) directly detected labels [4]. The detection based on the catalytic NPs employs a transformation of a substrate similar to traditional ELISA [5]. Comparing to ELISA, this process provides better stability and higher catalytic efficiency of nanomaterials such as AuNPs [6], Au@PdNPs [7], iron oxides NPs, Prussian blue NPs [8] or nanocomposite of PtNPs and graphene oxide [9].

The direct immunoassay readout (without the substrate catalysis) is usually based on luminescent labels. Nanomaterials such as quantum dots (QD) [10], carbon-based NPs [11], and photon-upconversion NPs [12] are used as an alternative to the conventional organic dyes and fluorescent proteins. The luminesce-based readout combines a high sensitivity with a simple and affordable instrumentation. Nevertheless, this readout method limits the range of possible labels to the materials exhibiting luminescent properties. Therefore, there is a demand for readout methods providing the universal detection of any label type that is independent on its catalytic or luminescent properties.

Laser-induced breakdown spectroscopy (LIBS) proved to be a suitable method for the NP detection in different matrices; ranging from the detection of QDs applied onto filter paper [13] to a detection of photon-upconversion NPs in the model organisms [14]. On top of that, the LIBS technique is abundantly used for mapping purposes, providing the lateral distribution of elements on the sample surface. This feature is used in a number of applications, for instance a mapping of NPs in mammal [15] and plant [16] tissues. The detection of NPs in aquatic suspensions [17, 18] or the detection of nano-powders in the polymer gels is well known. Also, the detection and characterization of single NPs by Optical Catapulting-Optical Trapping-LIBS (OC-OT-LIBS) [19] was already published. The pioneer LIBS study to detect the biomolecules labeled with CdTe or CdS QDs, followed by using aforementioned immunoassay readout was published by Konečná et al. [20]. On the other hand, the detection of small/scant volumes of liquid samples was studied only once using lab-on-a-chip devices designed especially for the LIBS interfacing [21].

To the best of our knowledge, the LIBS method as an alternative method of signal readout in immunochemical assays was investigated exclusively by Melikechi's research group [22], which also introduced the Tag-LIBS abbreviation [22]. The advanced Tag-femtosecond LIBS detection in microparticle-based immunochemical assays was demonstrated in a case study focused on the multi-element coded assay. The assay was carried out with Fe_2O_3 and TiO_2 microparticles bound to cancer antigen 125 via monoclonal antibodies [22].

In this work, two main experiments were carried out to prove LIBS to be a useful readout method for the common metal NPs-based immunoassays. The initial experiment focused on the most appropriate collection of Ag- and AuNPs plasma emission from the bottom of the standard 96-well microtiter plate and on the optimization of corresponding experimental conditions. The following experiment compared the LIBS method to the fluorescence readout in sandwich immunoassay where these methods are applied to detect the human serum albumin utilizing the label based on streptavidin-coated AgNPs.

Materials and methods

Chemicals and materials

The 20 nm colloid Ag NPs (the mean diameter of 19.9 nm) were obtained from BBI Solutions (www.bbisolutions.com; United Kingdom), 20 nm Au nanospheres citrate NanoXact™ (diameter of 18.9 ± 1.5 nm) were obtained from nanoComposix (www.nanocomposix.com; USA). Streptavidin-conjugated 40 nm AgNPs were purchased from Cytodiagnostics (www.cytodiagnostics.com; Canada). Biotin *N*-hydroxysuccinimide ester (NHS-biotin), bovine γ-globulin (BGG), bovine serum albumin (BSA), human serum albumin (HSA), *N*,*N*′-dimethylformamide (DMF), sodium azide, Tris, and Tween 20 were acquired from Sigma-Aldrich (www.sigmaaldrich.com; Germany). Ethylenediaminetetraacetic acid (EDTA) and glucose were purchased from Lachema (www.erbalachema.com; Czech Republic). Poly(vinyl alcohol) (PVA, 6 kDa) was purchased from Polysciences (www.polysciences.com; Germany). All other common chemicals were obtained in the highest quality available from Penta (www.pentachemicals.eu; Czech Republic). Anti-HSA mouse monoclonal antibody clone AL-01 was purchased from Exbio (www.exbio.cz; Czech Republic), fluorescein isothiocyanate (FITC)-labeled anti-HSA swine polyclonal antibody (AbF) was obtained from Sevapharma (sevapharma.czechtrade.us; Czech Republic).

Buffers used throughout this work were: phosphate buffer (PB; 50 mM NaH_2PO_4/Na_2HPO_4, pH 7.4), phosphate-buffered saline (PBS; PB + 150 mM NaCl), washing buffer (PB + 0.01% Tween 20, and 0.05% NaN_3), and assay buffer

(0.2% BSA, 0.5% BGG, 50 mM Tris, 150 mM NaCl, 5 mM EDTA, 0.2% PVA, 1% glucose, 0.05% NaN_3, and 0.01% Tween 20, pH 7.5).

Deposition of silver and gold nanoparticles in the microtiter plate

First, bare AgNPs and AuNPs were directly deposited on the bottom of the microtiter plate well and consequently ablated in order to optimize the LIBS experimental parameters. The deposition of NP suspensions to the microtiter plate well was performed using two approaches – manually and with an ink-jet deposition system.

For the manual formation of drops, selected volumes in a predetermined concentration were applied using a micropipette onto the bottom of each well. The drops dried at the air atmosphere and the laboratory temperature. The drop volumes were 10.0, 5.0, 2.5, 1.0, and 0.5 μL in the concentration provided by the supplier (AgNPs 3.08 $\mu g \cdot mL^{-1}$; AuNPs 53.0 $\mu g \cdot mL^{-1}$). Furthermore, the calibration plot was also measured for AgNPs, in a concentration range 3.08; 1.54; 0.77; 0.308; 0.205; 0.154 and 0.062 $\mu g \cdot mL^{-1}$ in a volume of 10 μL per one drop.

The ink-jet deposition was done using a piezo-driven non-contact dispensing system sciFLEXARRAYER S3 (www.scienion.com; Scienion, Germany). A 60 μm dispense capillary and the pulse parameters of 84 V, 50 μs and 500 Hz were used, resulting in a droplet volume of 250 pL. Four 1 μL drops were formed in each well of the microtiter plate by dispensing 4000 droplets onto each drop in 2 by 2 pattern with 2 mm spacing. The dilution series of AgNPs 3.08; 1.54; 0.77; 0.308; 0.154 and 0.077 $\mu g \cdot mL^{-1}$ were deposited and dried spontaneously.

Detection of nanoparticle labels in microtiter wells using laser-induced breakdown spectroscopy

Instrumentation and experimental settings

The LIBS measurements were done using the Sci-Trace (www.atomtrace.com; AtomTrace, Czech Republic) including the CageSystem as shown in Fig. 1a, b. The laser pulse (Nd:YAG laser LQ529A, www.solarlaser.com; Solar, Belarus; 532 nm, 10 ns) was used for material ablation (sampling). The laser pulse was focused to a tight spot (a crater diameter of 100 μm) and consequently a laser-induced plasma was created. A characteristic plasma emission was collected using a telescope and delivered via a 50 μm optical fiber to the entrance slit of an echelle spectrometer with a 200–975 nm wavelength range (Mechelle 5000 with the camera iStar 734i Andor, www.andor.oxinst.com; Oxford Instruments, UK). The software-controlled movement in *x,y,z* direction enabled scanning the bottoms of individual microtiter plate wells. The samples were measured in the air at the atmospheric pressure and laboratory temperature.

We first evaluated the possibility of a qualitative and a quantitative analysis of both types of selected nanoparticles – AgNPs and AuNPs – in a colinear LIBS arrangement. As mentioned before, the deposition to the microtiter plate was performed by two approaches – (i) manually and (ii) with an ink-jet printer. After drying, the analyses were done using experimental conditions which were optimized a priori. The settings used during the LIBS analysis were: 1.5 μs of the gate delay and 15 μs of the detection integration time, the laser pulse energy was set to 20 mJ. In case of manually (i) applied NPs, each bottom well area was analyzed in a raster of 15 × 15 spots with a 300 μm step as shown in Fig. 1c. After the ink-jet (ii) application of NPs, each bottom well area was analyzed in a raster of 30 × 30 spots with a 150 μm step. To ensure that no plasma emission was lost during the plasma collection from the 12 mm well depth was challenging. In order to handle this, a comparison experiment was carried out utilizing a dried AgNPs drop positioned the flat polystyrene surface (i.e. inverted microtiter plate).

Data processing

The most appropriate emission lines (represented in Fig. 2) of Ag I 338.31 nm (338.17–338.42 nm) and Au I 312.29 nm (312.20–312.34 nm) were selected and defined as the maximum line intensity with a proper background subtraction. The background was defined as the mean of the detected signal (338.54–338.79 nm for Ag and 312.40–312.54 nm for Au) near the selected analytical emission lines. The intensities were depicted as 2D maps representing the spatial distribution of the selected elements separately for each well. All signals for the selected emission line from 225 spectra were accumulated separately for each well after the manual applying of NPs. For the detection of NPs by applying the ink-jet system, 30 × 30 spots per one well with four dried drops were used. However, we only managed to accumulate the selected emission line from 225 spectra covering each drop separately (15 × 15 spots, a quarter of the well bottom). Thus, four accumulated signals of Ag I 338.31 nm emission line per one well were obtained. The accumulated signals were used in all following data evaluation. All LIBS data were processed using the AtomAnalyzer software (AtomTrace, Czech Republic) and visualized with OriginPro 2015 (www.originlab.com; OriginLab Corp., USA).

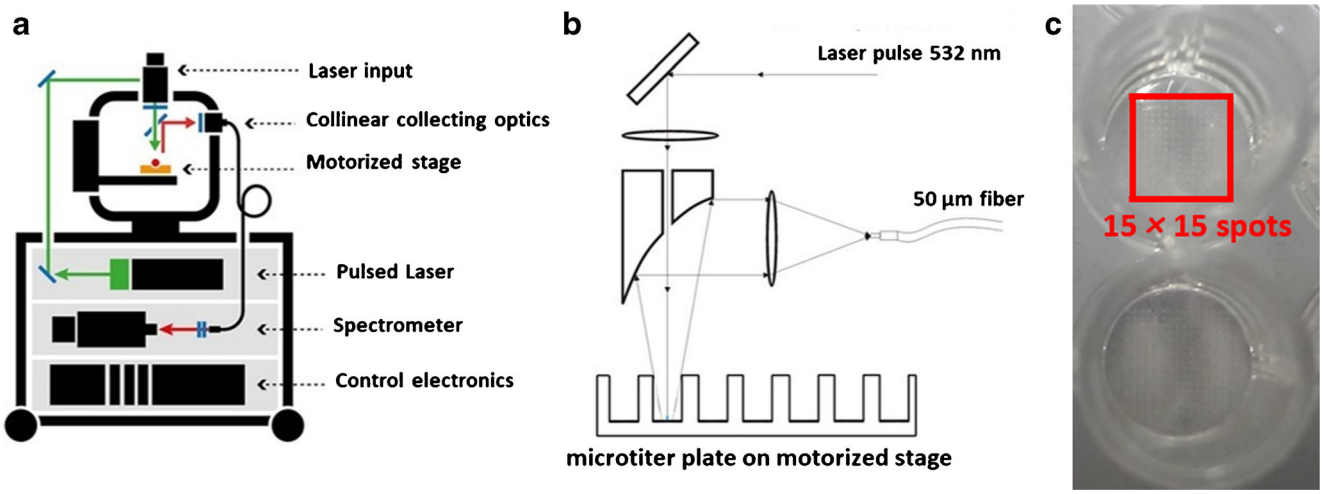

Fig. 1 **a** Scheme of Sci-Trace LIBS system; **b** Scheme of the plasma collection from the bottom of the standard 96-well microtiter plate in 12 mm depth; **c** Photograph of two wells of microtiter plate after LIBS measurements with highlighted area with raster of 15 × 15 ablation craters

Sandwich immunoassay for the detection of human serum albumin

Conjugation of detection antibody with biotin

A biotinylation of the detection antibody was done according to the protocol by Hermanson [23]. AbF was diluted in PBS to the concentration of 5 mg·mL^{-1} and NHS-biotin was dissolved in anhydrous DMF in the concentration of 20 mg·mL^{-1}. Subsequently, 20-times molar excess of NHS-biotin was added to the antibody and the mixture was incubated for 2 h at the room temperature. The AbF-biotin conjugate was purified using the Microcon centrifugal unit YM-100 (100 kDa MWCO; www.merckmillipore.com; Merck Millipore, USA) to PBS and stored at 4 °C in the concentration of 2 mg·mL^{-1}.

Sandwich immunoassay

A 96-well microtiter plate Nunc MaxiSorp (www.thermofisher.com; Thermo Fisher Scientific, USA) was coated with anti-HSA monoclonal antibody AL-01 (4 µg·mL^{-1} in PBS, 100 µL per well) and incubated overnight at 4 °C. All following incubations were carried out at the room temperature on a microplate shaker; after each step, the plate

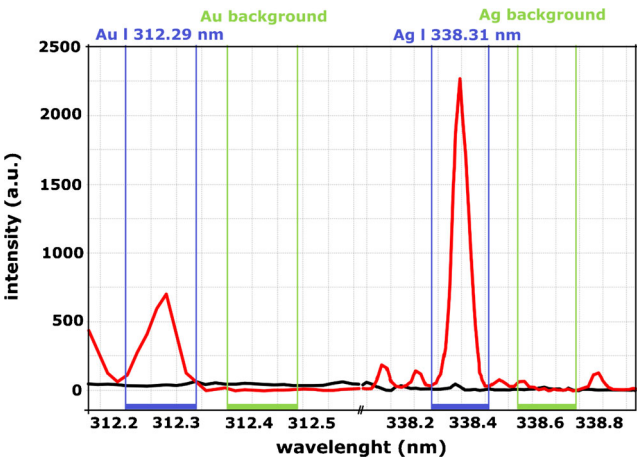

Fig. 2 Sample of spectra of AuNPs and AgNPs (red lines) and matrix (black lines) with highlighted parts of selected ranges of Au I 312.29 nm emission line (312.2–312.34 nm) together with background (312.4–312.54 nm) and Ag I 338.31 nm emission line (338.17–338.42 nm) together with background (338.54–338.79 nm)

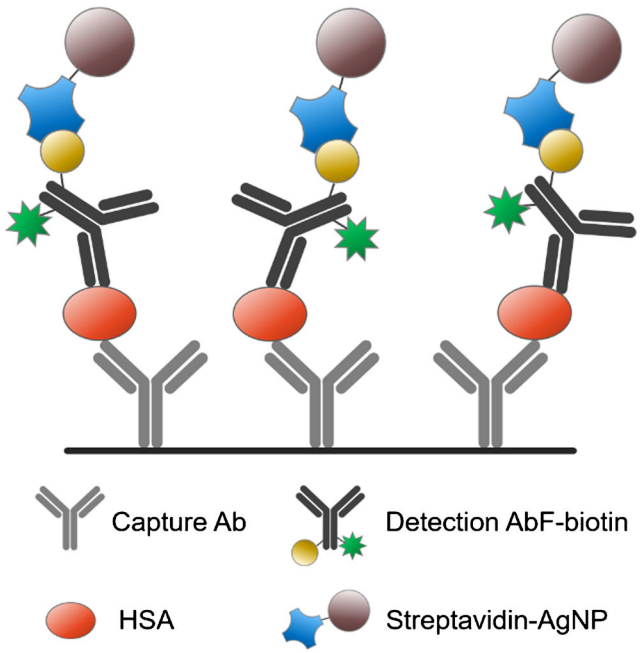

Fig. 3 A scheme of the sandwich immunocomplex in the detection of human serum albumin based on streptavidin-AgNP conjugate

was washed four times with 200 μL of washing buffer. The plate was blocked with 200 μL of 5% powdered milk (www.carlroth.com; Carl Roth, Germany) in PBS for 60 min. Subsequently, standard dilutions of HSA (10 ng·mL^{-1} to 100 μg·mL^{-1}) in the assay buffer were added (100 μL per well), and the plate was incubated for 60 min. Then, AbF-biotin conjugate in the assay buffer was added (the concentration equivalent to 100 μg·mL^{-1} of antibody, 100 μL per well) and incubated for 60 min. Finally, a conjugate of AgNPs with streptavidin (6 μg·mL^{-1}, 100 μL per well) was added for 60 min. After the last washing step, the wells were left empty and the scanning was performed in dry state, the protocol is based on our previously published methodology [8]. The scheme of the sandwich immunocomplex is shown in Fig. 3.

LIBS readout

The LIBS readout of the microtiter plate was based on the evaluation of the Ag I signal from the streptavidin-coated AgNP label. The experimental conditions remained the same as in case of the LIBS experiments with manually deposited nanoparticle drops. The gate delay was 1.5 μs, the detection integration time was 15 μs, the laser pulse energy was 20 mJ, and the raster of single pulses was 15 × 15 spots with a 300 μm step.

Fluorescence-based readout

To confirm the functionality of the sandwich immunoassay using a reference approach, the fluorescence of the AbF-biotin conjugate was measured using a Synergy 2 reader (www.biotek.com; BioTek, USA). A Tungsten lamp was used as an excitation source, with optics position *Top 510 nm*, the excitation and emission filters were set to 485 nm and 528 nm, respectively. The instrumental background corresponding to the average fluorescence of 12 unmodified wells was subtracted from the signals.

Results and discussion

LIBS detection of nanoparticles in the microtiter plate

Manual deposition of NPs to the microtiter plate

Firstly, the accumulated signal of Au I 312.29 nm emission line from 225 spectra covered a 10 μL drop (concentration 53.0 μg·mL^{-1}). The drop dried on the flat polystyrene surface (inverted microtiter plate). This accumulated signal was compared to accumulated signal values for identical AuNPs drops, which dried on the bottom of microtiter plate well. Differences between accumulated signals (5 replicates per one condition) showed to be lower than 5%. The accumulated signals from drops that dried on the flat surface were 332,000 ± 18,000 (a.u.) and accumulated signals from the spots inside the well were 319,000 ± 24,000 (a.u.). Moreover, a collection of plasma emissions from cavities, especially cylindrical, was shown to positively affect the signal repeatability and signal intensity. This influence was attributed to (i) the reflection and compression of the shock wave or to (ii) a more effective collection of plasma radiation caused by the reflection from the chamber walls as previously discussed [24]. The size of the cavities and the distance between the wall and plasma can affect the signal intensities. However, based on our data, we concluded that the plasma emission collection was not affected significantly during the plasma collection from the 12 mm depth and we continued with the LIBS detection from the bottom of a microtiter plate.

Secondly, the LIBS-based readout was used for a qualitative and quantitative determination of AgNP and AuNP suspensions applied with a micropipette onto the bottom of microtiter plate wells. The LIBS results are shown together in Fig. 4, the part (A) presents the accumulated signals of Ag I 338.31 nm for different concentrations of AgNPs (from 3.08 to 0.062 μg·mL^{-1}). The part (B) presents the accumulated signals of Ag I 338.31 nm for dried drops of five different volumes (10.0; 5.0; 2.5; 1.0 and 0.5 μL) of AgNPs in the concentration of 3.08 μg·mL^{-1}. The accumulated signals of Ag I 338.31 nm emission line recalculated to number of NPs on the bottom of the well for each drop are shown together in Fig. 4c. Figure 4d presents the accumulated signals of Au I 312.29 nm for drops of four different volumes (10.0; 5.0; 2.5 and 1.0 μL) of AuNPs in the concentration 53.0 μg·mL^{-1}. Maps representing 2D spatial distribution of AgNPs at the bottom of the well are depicted in Fig. 4 for selected concentrations (E) and volumes (F). It is clearly visible that NPs after manual deposition were non-homogeneously distributed due to the non-uniform drying of drops, which is well known [25].

The LOD for AgNPs (Ag I 338.31 nm) is 6.6·10^{6} NPs (291 pg Ag) and the LOD for AuNPs (Au I 312.29 nm) is 2.4·10^{8} NPs (16.1 ng Au). These values were calculated from the accumulated signals from well (raster consisted of 225 laser spots). Different LODs of Ag and Au, as well as the dependence of LODs of the element (Ag or Au) on a selected emission line, the sample matrix, and the concentration range of calibration plot was investigated in detail previously [26]. Furthermore, the well-known influence of the difference in the laser ablation process (single- or double-pulse ablation) was examined as described for the Au element [27]. The LODs for both elements were in the range from 0.4 to 94 ppm based on the experimental conditions [26, 27], which corresponds to

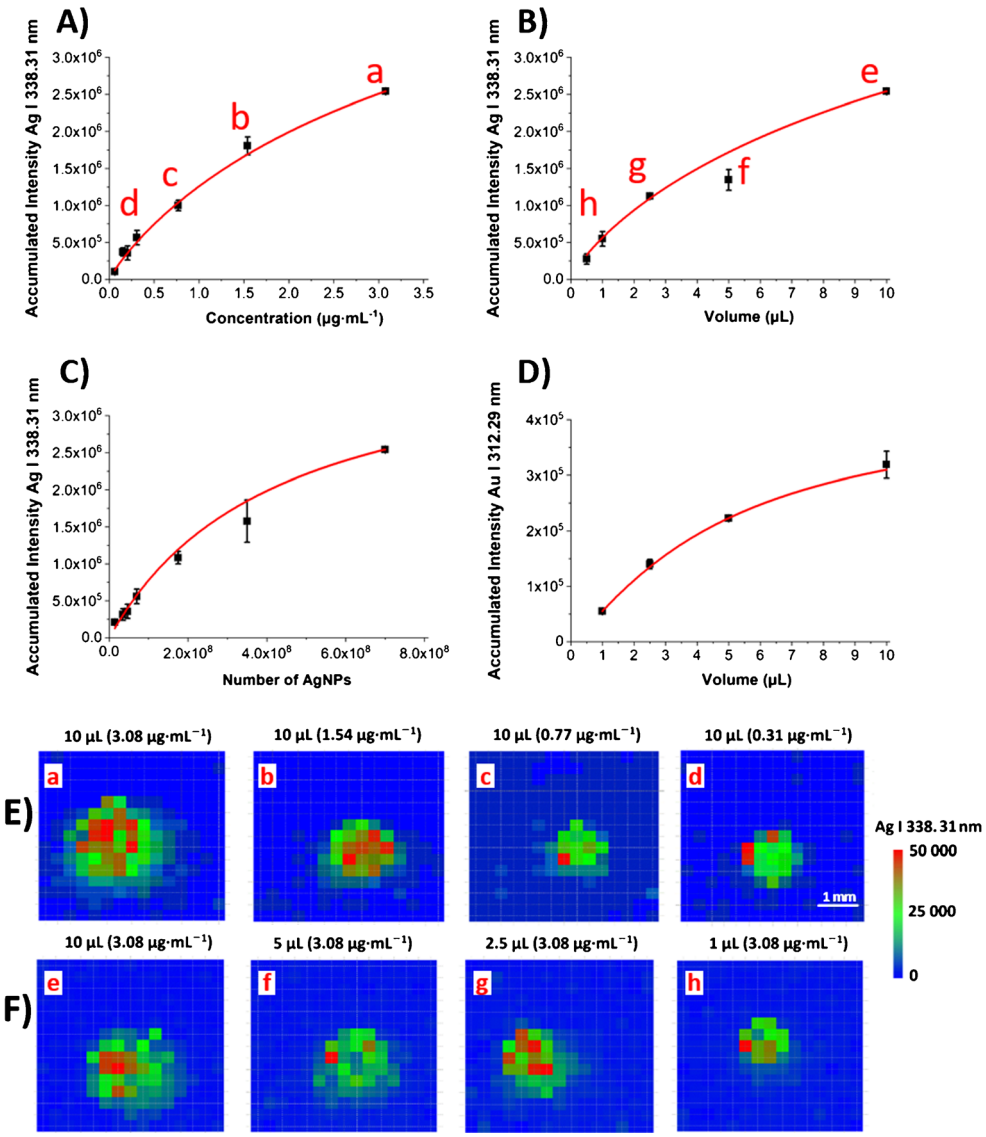

Fig. 4 Dependences of the LIBS accumulated Ag intensity on the concentration (**a**) and volume (**b**) of AgNPs; **c** both dependencies recalculated on the number of AgNPs shown together. **d** Dependency of the LIBS accumulated Au I intensity on the volume of AuNPs. Number of replicates $n = 4$. The symbols on the scatter plot represent mean values and SD as error bars. (**e**) LIBS maps constructed for Ag I 338.31 nm emission line of AgNPs dried drops of various concentration; **f** LIBS maps constructed for Ag I 338.31 nm emission line of AgNPs dried drops of various volumes. The scale bar shows 1 mm. Red letters (a-h) of selected LIBS maps are assigned to their accumulated signal values in graphs (**a**) and (**b**)

our results (Ag LOD 0.3 ppm for Ag I 338.31 nm and Au LOD 1.6 ppm for Au I 312.29 nm).

Overall, these LIBS results showed that the qualitative and quantitative analysis of both types of NPs is easy to implement and that the number of NPs (a different volume or different concentration applied to a microtiter plate well) is decisive for signal intensities. Due to the lower LODs, the AgNPs were used in all following experiments.

Ink-jet deposition of NPs to the microtiter plate

In this experiment, four 1 µL drops of AgNPs (the concentration range from 3.08 to 0.077 µg·mL^{-1}) were applied in each well of the microtiter plate using a 2 by 2 pattern with 2 mm spacing. The resulting dried drops were analyzed using LIBS. In comparison to the first LIBS experiment, one difference appeared. Due to the fact that the drops were of smaller size, the laser ablation step was reduced to 150 µm and the total number of laser spots from one well was 900 (30 × 30). The results are shown in Fig. 5, where the part A presents accumulated signals of Ag I 338.31 nm for six different concentrations (3.08; 1.54; 0.77; 0.308; 0.154 and 0.077 µg·mL^{-1}) of AgNPs in a volume of 1 µL per one drop. Also, this dependence of the accumulated signal on the concentration was fitted with Langmuir saturation curve. Furthermore, Fig. 5b depicts 2D maps of the spatial distribution of Ag I 338.31 nm emission line for four different concentrations (3.08; 1.54; 0.77; and 0.308 mg·L^{-1}) from one well.

The LOD for ink-jet deposited AgNPs was calculated again from the accumulated signals. In this case, the signals were not accumulated from the whole well bottom, but only from one quarter, which corresponded exactly to one drop

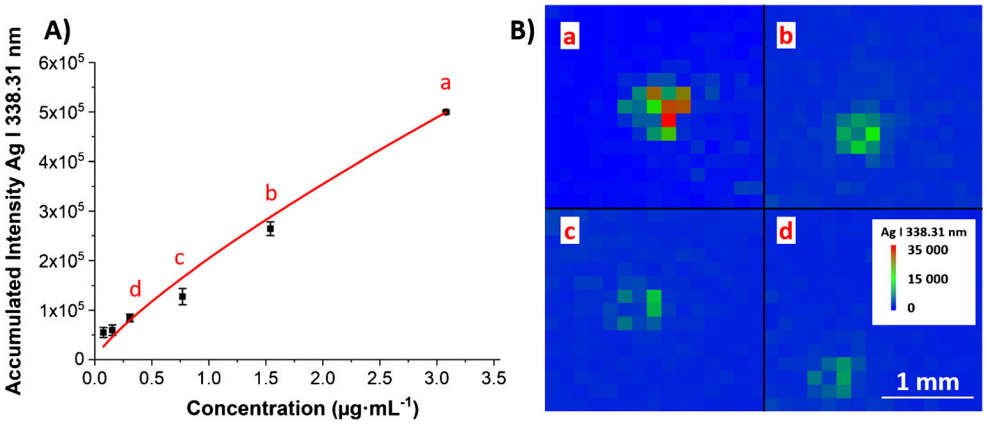

Fig. 5 **a** Dependency of accumulated Ag I 338.31 nm intensity on concentration of AgNPs. Number of replicates $n = 4$. The symbols on the scatter plot represent mean values and SD as error bars. **b** LIBS map constructed for Ag I 338.31 nm emission line of four drops (a: 3.08 µg·mL^{-1}, b: 1.54 µg·mL^{-1}, c: 0.77 µg·mL^{-1}, d: 0.308 µg·mL^{-1}) of AgNPs applied in a volume of 1 µL on the bottom of one well. The scale bar shows 1 mm

of NPs (15 × 15 spots from whole 30 × 30 spots from each well), as indicated in Fig. 5b by black cross lines. The LOD for AgNPs (Ag I 338.31 nm) is $6.7 \cdot 10^6$ NPs (293 pg Ag). The LODs for AgNPs from both experiments were very similar, 291 pg Ag (manual deposition) and 293 pg Ag (ink-jet system). This situation points to the robustness of LIBS method, in case that none of the previously mentioned parameters such as the matrix of samples, and the selected emission line of element or ablation process is changed. The method of NP deposition had no influence on the signal detection and consequently had no influence on LODs. In comparison to the manual application of NPs dispersion with micropipette, the speed, accuracy, and repeatability of the ink-jet system application need to be highlighted together with the space saving and possibility of multiplexing (multiple drops per one well). Considering the following application as a label for immunoassay, the ink-jet deposition resulted in the signal being nearly linearly dependent on the AgNP concentration (Fig. 5a), which was not the case for the manual deposition (Fig. 4a). The linear dependence of the signal on the bound label amount is advantageous as it does not complicate the interpretation of non-linear immunoanalytical calibration plots.

Sandwich immunoassay for detection of human serum albumin

The optimized LIBS-based readout was used for a determination of streptavidin-coated AgNPs as a label in the sandwich HSA detection. The sandwich assay for HSA was optimized in our previous work [8], therefore we focused here on the optimization of the labeling steps. We analyzed the concentrations of HSA in the range from 10 ng·mL^{-1} to 100 µg·mL^{-1}. The results are shown in Fig. 6, together with their comparison to the reference readout based on the fluorescence of a conjugate of detection antibody with FITC and biotin. All curves were fitted by a four-parameter logistic function. For the lower concentration of streptavidin-coated AgNPs of 3 µg·mL^{-1}, LIBS provided lower sensitivity than the fluorescence-based readout. However, when the concentration of streptavidin-AgNP label was increased to 6 µg·mL^{-1}, the LIBS reached a sensitivity comparable to the fluorescence-based readout. Both

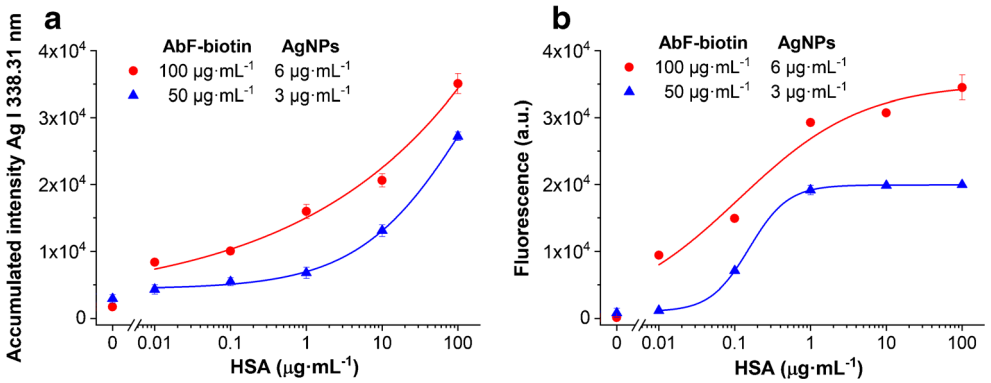

Fig. 6 **a** Dependences of LIBS accumulated Ag I 338.31 nm intensity on HSA concentration; **b** Dependences of fluorescence signal on HSA concentration. Number of replicates $n = 4$. The symbols on the scatter plot represent mean values and SD as error bars

methods provided a detection limit of 10 ng·mL^{-1} of HSA ($S/N > 3$). Compared to the fluorescence readout where plateau was reached at 1 μg·mL^{-1} of HSA, LIBS offered wider working range up to 100 μg·mL^{-1}. This is a significant advantage considering e.g. the levels typical for albuminuria.

The previous reports about LIBS being used to provide a readout of antibody-based assays are very sparse. Markushin et al. (2015) previously employed femtosecond LIBS for a detection of cancer antigen 125 with LOD of 0.01 U·mL^{-1} [22]. However, the assay was limited because it was necessary to use magnetic particles for an antigen capture, followed by a deposition of resulting sandwich immunocomplexes on the filter paper. Whereas, the system here allows scanning the standard polystyrene microtiter plates without the necessity to significantly change the routine assay procedure. Unfortunately, due to the different experimental settings, different ablation process, various analyte (and units expressed as U·mL^{-1}), the sensitivity of the two approaches cannot be directly compared.

Considering some other approaches, Raman spectroscopy, especially Surface-Enhanced Raman Scattering (SERS) [28, 29], and Inductively Coupled Plasma Mass Spectrometry (ICP-MS) [30] showed to be useable to detect various NPs labels in immunoassays. Quantum dots or metal-doped NPs served as labels for a detection of carcinoembryonic antigen [31], allergens in food [32], or a multiplexed detection of C-reactive protein, alpha-fetoprotein, and neuron-specific enolase [33] by ICP-MS readout method. In comparison of ICP-MS to LIBS, several disadvantages of ICP-MS have to be mentioned, including high cost of instrumentation, high operation costs, high demands on vacuum environment, and a long duration of analysis. On the other hand, SERS showed to be useable for a detection of various labels, so-called SERS-nanotags, in various biosensing of proteins, nucleic acids, and many others, as summarized in a previously published review [34]. Many advantages as the high sensitivity, specificity, multiplexing capability, photostability of SERS-nanotags, and low detection limits (down to the femtomolar level) are compensated by the need of special SERS-nanotags. In contrast, LIBS can detect various commonly used NPs.

Conclusion

We presented Tag-LIBS with nanosecond laser ablation process of sampling as a universal readout method for the immunoassays based on nanoparticle labels. An innovative arrangement of the collinear plasma collection and the focusing optics for LIBS was developed in order to enable a detection of NPs directly in a standard microtiter plate. Using this LIBS setup, we demonstrated the capability to detect AuNPs and AgNPs with a detection limit of $6.6 \cdot 10^6$ and $2.4 \cdot 10^8$ particles for AgNPs and AuNPs, respectively. The LIBS detection of the dried drops on the bottom of a microtiter plate was more appropriate for the drops deposited with the ink-jet system.

The optimized LIBS setup was used for the readout of sandwich immunoassay with streptavidin-coated AgNPs as a label. Human serum albumin, a diagnostic marker of albuminuria, was detected with a LOD of 10 ng·mL^{-1}, which is nearly comparable with the sensitivity of the fluorescence-based readout. Both techniques are complementary readout methods. The fluorescence detection showed a slightly better sensitivity but a substantial tendency to saturation, on the other hand, LIBS presents wider dynamic range, as it is obvious from the immunoassay results. The great LIBS advantage is the fast analysis time, the possibility of a multi-elemental (multi-biomarker) analysis, and the possibility to detect NPs without any photoluminescence or without any effect of potential NPs photoluminescence quenching. Furthermore, LIBS method does not show the broadband interfering spectral emissions.

We expect that Tag-LIBS described here can be applied to detect many types of biomarkers in nanoparticle-based immunochemical assays. It can also be used for a parallel detection of a multiple set of biomarkers in the near future. Moreover, we would like to emphasize the possibility to combine four readout methods (LIBS, SERS, Raman spectroscopy, and fluorescence detection) for their similar detection principles in one optical reader. This multiplexed readout represents a novel strategy for a robust simultaneous determination of various elements, chemical bonds, special nanotags, and fluorescent substances. Thus, this is going to be a subject of our future work.

Acknowledgments This research has been financially supported by the Ministry of Education, Youth and Sports of the Czech Republic under the project CEITEC 2020 (LQ1601). This work was also carried out with the support of CEITEC Nano Research Infrastructure (MEYS CR, 2016–2019), CEITEC Nano+ project, ID CZ.02.1.01/0.0/0.0/16_013/0001728. CIISB research infrastructure project LM2015043, funded by MEYS CR, is gratefully acknowledged for financial support of the measurements at CF Nanobiotechnology.

Compliance with ethical standards The author(s) declare that they have no competing interests.

References

1. Tighe PJ, Ryder RR, Todd I, Fairclough LC (2015) ELISA in the multiplex era: potentials and pitfalls. Proteomics Clin Appl 9:406–422. https://doi.org/10.1002/prca.201400130
2. Lequin RM (2005) Enzyme immunoassay (EIA)/enzyme-linked immunosorbent assay (ELISA). Clin Chem 51:2415–2418. https://doi.org/10.1373/clinchem.2005.051532

3. Wei H, Wang E (2013) Nanomaterials with enzyme-like characteristics (nanozymes): next-generation artificial enzymes. Chem Soc Rev 42:6060–6093. https://doi.org/10.1039/c3cs35486e
4. Farka Z, Juřík T, Kovář D, Trnková L, Skládal P (2017) Nanoparticle-based immunochemical biosensors and assays: recent advances and challenges. Chem Rev 117:9973–10042. https://doi.org/10.1021/acs.chemrev.7b00037
5. Wu J, Li S, Wei H (2018) Multifunctional nanozymes: enzyme-like catalytic activity combined with magnetism and surface plasmon resonance. Nanoscale Horizons 3:367–382. https://doi.org/10.1039/c8nh00070k
6. Sang F, Liu J, Zhang X, Pan J (2018) An aptamer-based colorimetric Pt(II) assay based on the use of gold nanoparticles and a cationic polymer. Microchim Acta 185:1–7. https://doi.org/10.1007/s00604-018-2794-6
7. Dehghani Z, Hosseini M, Mohammadnejad J, Bakhshi B, Rezayan AH (2018) Colorimetric aptasensor for campylobacter jejuni cells by exploiting the peroxidase like activity of Au@Pd nanoparticles. Microchim Acta 185:448. https://doi.org/10.1007/s00604-018-2976-2
8. Farka Z, Čunderlová V, Horáčková V, Pastucha M, Mikušová Z, Hlaváček A, Skládal P (2018) Prussian blue nanoparticles as a catalytic label in a Sandwich Nanozyme-linked immunosorbent assay. Anal Chem 90:2348–2354. https://doi.org/10.1021/acs.analchem.7b04883
9. Xu HH, Deng HH, Lin XQ, Wu YY, Lin XL, Peng HP, Liu AL, Xia XH, Chen W (2017) Colorimetric glutathione assay based on the peroxidase-like activity of a nanocomposite consisting of platinum nanoparticles and graphene oxide. Microchim Acta 184:3945–3951. https://doi.org/10.1007/s00604-017-2429-3
10. Wu Y-T, Qiu X, Lindbo S, Susumu K, Medintz IL, Hober S, Hildebrandt N (2018) Quantum dot-based FRET immunoassay for HER2 using Ultrasmall affinity proteins. Small 14:1802266. https://doi.org/10.1002/smll.201802266
11. Yang L, Deng W, Cheng C, Tan Y, Xie Q, Yao S (2018) Fluorescent immunoassay for the detection of pathogenic Bacteria at the single-cell level using carbon dots-encapsulated breakable Organosilica Nanocapsule as labels. ACS Appl Mater Interfaces 10:3441–3448. https://doi.org/10.1021/acsami.7b18714
12. Farka Z, Mickert MJ, Hlaváček A, Skládal P, Gorris HH (2017) Single molecule upconversion-linked immunosorbent assay with extended dynamic range for the sensitive detection of diagnostic biomarkers. Anal Chem 89:11825–11830. https://doi.org/10.1021/acs.analchem.7b03542
13. Škarková P, Novotný K, Lubal P, Jebavá A, Pořízka P, Klus J, Farka Z, Hrdlička A, Kaiser J (2017) 2d distribution mapping of quantum dots injected onto filtration paper by laser-induced breakdown spectroscopy. Spectrochim Acta - Part B At Spectrosc 131:107–114. https://doi.org/10.1016/j.sab.2017.03.016
14. Modlitbová P, Hlaváček A, Švestková T, et al (2019) The effects of photon-upconversion nanoparticles on the growth of radish and duckweed: bioaccumulation, imaging, and spectroscopic studies. Chemosphere 225:723–734. https://doi.org/10.1016/j.chemosphere.2019.03.074
15. Gimenez Y, Busser B, Trichard F, Kulesza A, Laurent JM, Zaun V, Lux F, Benoit JM, Panczer G, Dugourd P, Tillement O, Pelascini F, Sancey L, Motto-Ros V (2016) 3D imaging of nanoparticle distribution in biological tissue by laser-induced breakdown spectroscopy. Sci Rep 6:1–9. https://doi.org/10.1038/srep29936
16. Modlitbová P, Novotný K, Pořízka P, Klus J, Lubal P, Zlámalová-Gargošová H, Kaiser J (2018) Comparative investigation of toxicity and bioaccumulation of Cd-based quantum dots and Cd salt in freshwater plant *Lemna minor* L. Ecotoxicol Environ Saf 147:334–341. https://doi.org/10.1016/j.ecoenv.2017.08.053
17. Sovago M, Buis EJ, Sandtke M (2013) Nanoparticle detection in aqueous solutions using Raman and laser induced breakdown spectroscopy. Spectrochim Acta - Part B At Spectrosc 87:182–187. https://doi.org/10.1016/j.sab.2013.05.033
18. Borowik T, Przybyło M, Pala K, Otlewski J, Langner M (2011) Quantitative measurement of Au and Fe in ferromagnetic nanoparticles with laser induced breakdown spectroscopy using a polymer-based gel matrix. Spectrochim Acta - Part B At Spectrosc 66:726–732. https://doi.org/10.1016/j.sab.2011.09.008
19. Fortes FJ, Fernández-Bravo A, Javier Laserna J (2014) Chemical characterization of single micro- and nano-particles by optical catapulting-optical trapping-laser-induced breakdown spectroscopy. Spectrochim Acta - Part B At Spectrosc 100:78–85. https://doi.org/10.1016/j.sab.2014.08.023
20. Konecna M, Novotny K, Krizkova S, Blazkova I, Kopel P, Kaiser J, Hodek P, Kizek R, Adam V (2014) Identification of quantum dots labeled metallothionein by fast scanning laser-induced breakdown spectroscopy. Spectrochim Acta - Part B At Spectrosc 101:220–225. https://doi.org/10.1016/j.sab.2014.08.037
21. Metzinger A, Nagy A, Gáspár A, Márton Z, Kovács-Széles É, Galbács G (2016) The feasibility of liquid sample microanalysis using polydimethylsiloxane microfluidic chips with in-channel and in-port laser-induced breakdown spectroscopy detection. Spectrochim Acta Part B At Spectrosc 126:23–30. https://doi.org/10.1016/j.sab.2016.10.014
22. Markushin Y, Sivakumar P, Connolly D, Melikechi N (2015) Tag-femtosecond laser-induced breakdown spectroscopy for the sensitive detection of cancer antigen 125 in blood plasma. Anal Bioanal Chem 407:1849–1855. https://doi.org/10.1007/s00216-014-8433-0
23. Hermanson G (2013) Bioconjugate Techniques, 3rd edn. Academic Press
24. Li Y, Tian D, Ding Y, Yang G, Liu K, Wang C, Han X (2018) A review of laser-induced breakdown spectroscopy signal enhancement. Appl Spectrosc Rev 53:1–35. https://doi.org/10.1080/05704928.2017.1352509
25. Park BS, Jung KI, Lee SJ, Lee KY, Jung HW (2018) Effect of particle shape on drying dynamics in suspension drops using multi-speckle diffusing wave spectroscopy. Colloid Polym Sci 296:971–979. https://doi.org/10.1007/s00396-018-4315-x
26. Díaz D, Hahn DW, Molina A (2017) Spectrochimica Acta Part B Quanti fi cation of gold and silver in minerals by laser-induced breakdown spectroscopy. Spectrochim Acta Part B At Spectrosc 136:106–115. https://doi.org/10.1016/j.sab.2017.08.008
27. Rifai K, Laville S, Vidal F, Sabsabi M, Chaker M (2012) Quantitative analysis of metallic traces in water-based liquids by UV-IR double-pulse laser-induced breakdown spectroscopy. J Anal At Spectrom 27:276–283. https://doi.org/10.1039/c1ja10178a
28. Liu R, Liu B, Guan G, Jiang C, Zhang Z (2012) Multilayered shell SERS nanotags with a highly uniform single-particle Raman readout for ultrasensitive immunoassays. Chem Commun 48:9421–9423. https://doi.org/10.1039/c2cc34115h
29. Wang Y, Vaidyanathan R, Shiddiky MJA, Trau M (2015) Enabling rapid and specific surface-enhanced Raman scattering immunoassay using Nanoscaled surface shear forces. ACS Nano 9:6354–6362. https://doi.org/10.1021/acsnano.5b01929
30. Quinn ZA, Baranov VI, Tanner SD, Wrana JL (2002) Simultaneous determination of proteins using an element-tagged immunoassay coupled with ICP-MS detection. J Anal At Spectrom 17:892–896. https://doi.org/10.1039/b202306g
31. Cao Y, Mo G, Feng J, He X, Tang L, Yu C, Deng B (2018) Based on ZnSe quantum dots labeling and single particle mode ICP-MS coupled with sandwich magnetic immunoassay for the detection of carcinoembryonic antigen in human serum. Anal Chim Acta 1028:22–31. https://doi.org/10.1016/j.aca.2018.04.039

32. Careri M, Elviri L, Mangia A, Mucchino C (2007) ICP-MS as a novel detection system for quantitative element-tagged immunoassay of hidden peanut allergens in foods. Anal Bioanal Chem 387: 1851–1854. https://doi.org/10.1007/s00216-006-1091-0
33. Ko JA, Lim HB (2016) Metal-doped inorganic nanoparticles for multiplex detection of biomarkers by a sandwich-type ICP-MS immunoassay. Anal Chim Acta 938:1–6. https://doi.org/10.1016/j.aca.2016.07.035
34. Zhang W, Jiang L, Piper JA, Wang Y (2018) SERS Nanotags and their applications in biosensing and bioimaging. J Anal Test 2:26–44. https://doi.org/10.1007/s41664-018-0053-9